1.4 Effects of Small Vibrations on Marangoni Convection in a Liquid Bridge and Numerical Simulation of Surface Oscillation

Masahiro Kawaji
University of Toronto

EFFECTS OF SMALL VIBRATIONS ON MARANGONI CONVECTION IN A LIQUID BRIDGE AND NUMERICAL SIMULATION OF SURFACE OSCILLATION

R.Q. Liang, M. N.-Esfahany and M. Kawaji

Dept. of Chemical Engineering and Applied Chemistry, 200 College Street, Toronto, Ontario M5S 3E5, Canada

ABSTRACT

The effects of small vibrations on Marangoni convection were investigated using a liquid bridge of 5 cSt silicone oil with a disk diameter of 7.0 mm, and an aspect ratio close to 0.5. Experiments were performed to determine the critical temperature difference data for no vibration case and with small vibrations applied. The surface oscillation amplitude was also determined experimentally, and a 3-D numerical simulation model was developed using a level set algorithm to predict the surface oscillations of an isothermal liquid bridge. The experimental results have shown that the effect of small vibrations on the onset of oscillatory flow is small since the critical temperature difference data for different aspect ratios were not affected by the vibrations. This is consistent with the results obtained for acetone bridges reported in the previous year.

The peak amplitudes of surface oscillations decreased as the disk temperature difference was increased and the average liquid temperature decreased. This can be attributed to an increase in surface tension which stabilizes the liquid bridge surface. The surface oscillation amplitude, however, showed an abrupt increase at the onset of oscillatory Marangoni convection, and then a decrease as the temperature difference was further increased above the critical value. The reason for this variation in the surface oscillation amplitude with the temperature difference is unclear and needs to be investigated further.

To clarify the surface oscillation phenomena induced by external vibrations, experiments and numerical simulations were conducted for an isothermal silicone oil bridge of 7.0 mm diameter. By subjecting the liquid bridge to small random vibrations, the surface oscillation frequency could be clearly determined. The computational results have also shown a similar surface oscillation frequency.

1. INTRODUCTION

Marangoni convection in liquid bridges changes from a steady, axi-symmetric flow to an oscillatory flow, when a large temperature gradient is imposed. Such an oscillation in flow can lead to non-uniformities in crystal structure such as striations[1,2] when a floating zone process is used to fabricate single semiconductor crystals of high purity from melts. Large liquid bridges can be formed under microgravity in space, however, the liquid bridges are also susceptible to small vibrations or g-jitter on space platforms that may excite oscillations of the free surface and add to the complexity of the hydrodynamics involved.

The effects of small horizontal vibrations on the critical temperature difference and surface oscillation of acetone liquid bridges were previously investigated experimentally.[3, 4] Also, a *horizontal vibration model* of Ichikawa et al.[5] was adopted to predict the resonance vibration frequency of an isothermal liquid bridge.

In this work, the effects of small vibrations on the critical temperature difference and surface oscillation amplitudes were investigated for liquid bridges of 5 cSt silicone oil. The surface oscillation characteristics of isothermal silicone oil bridges were also investigated experimentally and numerically.

2. EXPERIMENTAL APPARATUS AND INSTRUMENTATION

A schematic of the test section is shown in Figure 2.1. It had upper and lower disks of 7.0 mm diameter made of brass. Details of the experimental apparatus and procedure can be found in previous reports.[4,6] A PC-controlled vibration stage (Parker-Daedal Model 404XR150MP) was employed to apply horizontal vibrations to a liquid bridge and find the effect on ΔT_{cr} and the response of the free surface. The test section was mounted on the stage, which was translated horizontally at a constant speed. Due to friction effects, small vibrations were experienced by the liquid bridge in all directions. A video camera and a single-axis accelerometer were mounted on the same stage to monitor the liquid bridge motion and acceleration level, respectively.

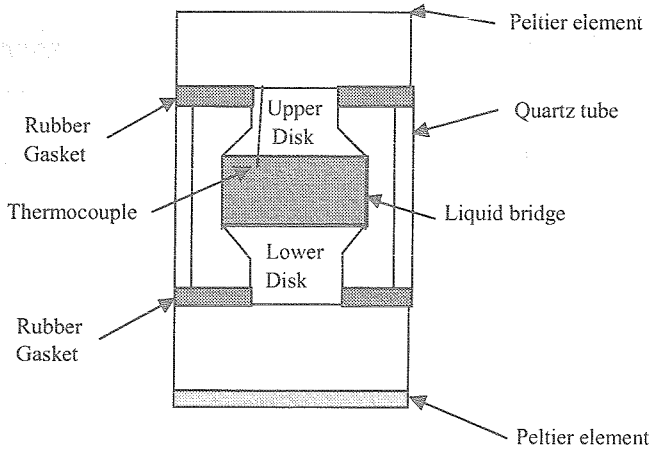

Figure 2.1 Schematic of the test section

3 NUMERICAL SIMULATION

Tracking or capturing a moving free surface in numerical simulation has been an important research field for more than a decade. In practice, however, the numerical simulations of free surface flows are difficult, especially if the free surface separates fluids of dramatically different densities. So far, the approaches available for treating moving interfaces include Lagrangian methods, such as boundary-fitted grid and boundary-integral methods, and Eulerian methods, such as volume of fluid, level set, and enthalpy methods. As a new Eulerian method, the level set method was originally introduced by Osher and Sethian,[7] and has been widely applied to a variety of free surface flows.[8, 9, 10] Unlike the VOF method, which divides the spatial domain into cells that contain fractions of material, the level set method divides the domain into grid points. Each point contains the value of the level set function at that point, therefore, there is an entire family of contours. By updating the value of level set at each grid point, a new entire family of contours will be given and only one of which is the zero level set, which corresponds to the interface. The major merit of this method is that it naturally constructs the fundamental solution to interface propagation. However, there has been no modeling work done on Marangoni convection using the level set method in the literature. In this work, the level set method has been adopted to capture the three dimensional motion of a vibrating free surface in a liquid bridge driven by small horizontal vibrations.

3.1 3-D Governing Equations

The equations of motion for incompressible flow including gravitational and small horizontal acceleration forces, viscous, and surface tension effects are given by the incompressible Navier-Stokes equations. These may be expressed as

$$\frac{\partial u}{\partial x}+\frac{\partial v}{\partial y}+\frac{\partial w}{\partial z}=0 \tag{1}$$

$$\frac{\partial u}{\partial t}=-u\frac{\partial u}{\partial x}-v\frac{\partial u}{\partial y}-w\frac{\partial u}{\partial z}+FGX+\frac{1}{\rho}\left(-\frac{\partial p}{\partial x}+\frac{\mu}{\mathrm{Re}}\left(\frac{\partial^2 u}{\partial x^2}+\frac{\partial^2 u}{\partial y^2}+\frac{\partial^2 u}{\partial z^2}\right)+\frac{1}{We}\kappa\delta(d)\mathbf{n}\right) \tag{2}$$

$$\frac{\partial v}{\partial t}=-u\frac{\partial v}{\partial x}-v\frac{\partial v}{\partial y}-w\frac{\partial v}{\partial z}+\frac{1}{\rho}\left(-\frac{\partial p}{\partial y}+\frac{\mu}{\mathrm{Re}}\left(\frac{\partial^2 v}{\partial x^2}+\frac{\partial^2 v}{\partial y^2}+\frac{\partial^2 v}{\partial z^2}\right)+\frac{1}{We}\kappa\delta(d)\mathbf{n}\right) \tag{3}$$

$$\frac{\partial w}{\partial t}=-u\frac{\partial w}{\partial x}-v\frac{\partial w}{\partial y}-w\frac{\partial w}{\partial z}+\frac{1}{Fr^2}+\frac{1}{\rho}\left(-\frac{\partial p}{\partial z}+\frac{\mu}{\mathrm{Re}}\left(\frac{\partial^2 w}{\partial x^2}+\frac{\partial^2 w}{\partial y^2}+\frac{\partial^2 w}{\partial z^2}\right)+\frac{1}{We}\kappa\delta(d)\mathbf{n}\right) \tag{4}$$

where, $FGX=\dfrac{g_x\bar{L}}{U_\infty^2}$, $g_x=A\omega^2\sin\omega t$, $\omega=2\pi f$

The dimensionless parameters used are Reynolds number, Froude number, and Weber number, respectively. $\mathrm{Re}=\frac{\rho_l \bar{L} U_\infty}{\mu_l}$, $Fr=\sqrt{\frac{u_\infty^2}{g\bar{L}}}$, $We=\frac{\rho_l \bar{L} U_\infty^2}{\sigma}$

3.2 Level Set Method

3.2.1 Level set function and its formulation

Briefly, the level set function is a signed normal distance from the interface. In Figure 3.1 we consider a closed moving interface Γ(t) propagating with speed F normal to itself, and Ω(t) is the region that Γ(t) encloses. We associate Ω(t) with an auxiliary function $\phi(\mathbf{x},t)$, which is called the level set function,

$$\phi(\mathbf{x},t)=\begin{cases} dist(\mathbf{x},\Gamma(t),t) & if\ \mathbf{x}\ \ outside\ \ \Gamma(t) \\ -dist(\mathbf{x},\Gamma(t),t) & if\ \mathbf{x}\ \ inside\ \ \Gamma(t) \end{cases} \tag{5}$$

$$\Gamma(t)=\{\mathbf{x}\in\Omega:\phi(\mathbf{x},t)=0\} \tag{6}$$

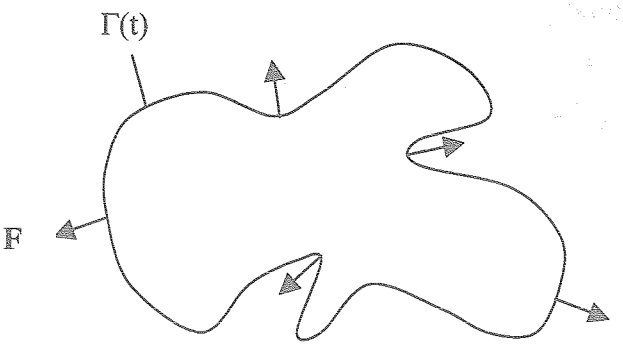

Figure 3.1 An interface propagating with a speed of F

As a nice feature of the level set method, the unit normal vector of the interface n and normal speed F can be simply represented in terms of $\phi(\mathbf{x},t)$

$$\mathbf{n}=-\frac{\nabla\phi}{|\nabla\phi|} \tag{7}$$

$$\mathbb{F}=\frac{\phi_t}{|\nabla\phi|} \tag{8}$$

If the flow velocity is given by $\mathbf{u}(\mathbf{x},t)$, we have

$$\mathbf{u}\,\mathbf{gn}=\mathbb{F} \tag{9}$$

From equations (7) and (9), we have

$$\phi_t+\mathbf{ug}\nabla\phi=\phi_t-\mathbf{ugn}|\nabla\phi|=\phi_t-\mathbb{F}|\nabla\phi| \tag{10}$$

From equation (8), we have

$$\phi_t - \mathbb{F}|\nabla\phi| = 0 \tag{11}$$

So, from equations (10) and (11) we get

$$\phi_t + \mathbf{u}\mathbf{g}\nabla\phi = 0 \tag{12}$$

Equation (12) is called the level set equation. This equation will move the zero level of ϕ exactly as the actual interface moves.

3.2.2 Re-initialization of level set function

Because we initialize the level set function ϕ as a signed distance from the interface, we have

$$|\nabla\phi| = 1 \tag{13}$$

When we move the level set function ϕ with equation (12), ϕ will no longer be a distance function and may become irregular at later times.

$$|\nabla\phi| \neq 1 \tag{14}$$

This will necessarily result in the variation of interface thickness in time, making further computation and contour plotting highly inaccurate. Fortunately, we can ignore all values of ϕ far from the zero level set and replace the solution ϕ at any time by another function ϕ_0 with the same zero set as ϕ and then take ϕ_0 as the initial data to use. An iterative procedure was proposed to fulfill the above process. [11]

$$\phi_t = sign(\phi_0)\left(1 - |\nabla\phi|\right) \tag{15}$$

$$\phi(\mathbf{x}, 0) = \phi_0(\mathbf{x}) \tag{16}$$

The stopping criterion for the iteration is

$$E = \frac{\sum_{|\phi^m_{i,j,k}| < A} \left|\phi^{m+1}_{i,j,k} - \phi^m_{i,j,k}\right|}{M} < (\Delta t)(\Delta x)^2 \tag{17}$$

Here, M = number of grid points where $\left|\phi^m_{i,j,k}\right| < A$, $A = 3\Delta x / 4$, and we adopted the above procedure to re-initialize the level set function.

3.2.3 An improvement on re-initialization of level set function

By carrying out re-initialization, the level set function will remain a distance function at later times, and will ensure the interface having a finite thickness all the time. Another important issue is mass conservation. For incompressible flows, the total mass must be conserved in time. However, just like other Eulerian methods, such as the VOF method, even with the above

re-initialization procedure, it has been found that the total mass is not completely conserved in time. To overcome this difficulty, an improvement has been firstly made on the re-initialization procedure aimed at preserving the total mass in time. We classify the grid points into two groups: the first group includes the grid points that are the closest to the interface and on the interface, and the other grid points belong to the second group. For simplicity, let us consider a 2-D domain, if any one of the following

$$\left(\phi_{i,j}\right)\left(\phi_{i,j+1}\right)\le 0 \tag{18}$$

$$\left(\phi_{i,j}\right)\left(\phi_{i,j-1}\right)\le 0 \tag{19}$$

$$\left(\phi_{i,j}\right)\left(\phi_{i+1,j}\right)\le 0 \tag{20}$$

$$\left(\phi_{i,j}\right)\left(\phi_{i-1,j}\right)\le 0 \tag{21}$$

is satisfied, (i,j) belongs to the first group points, otherwise, (i,j) belongs to the second group points. For the first group points, we solve the convection equation $\phi_t+(\mathbf{u}\mathrm{g}\nabla)\phi=0$ and denote the updated ϕ by $\phi^{(n+1)}$. We have now advanced one time step. The zero level sets of ϕ^{n+1} give the new interface points and ϕ^{n+1} is a distance function. For the second group points, we solve the convection equation $\phi_t+(\mathbf{u}\mathrm{g}\nabla)\phi=0$ and denote the updated ϕ by $\phi^{(n+1/2)}$, and then construct a new distance function by solving $\phi_t=S\left(\phi^{(n+1/2)}\right)\left(1-|\nabla\phi|\right)$ with $\phi(\mathrm{x},0)=\phi^{(n+1/2)}(\mathrm{x})$ to steady state. We denote the steady state solution by ϕ^{n+1} and we have now advanced one time step. The zero level sets of ϕ^{n+1} give the new interface points and ϕ^{n+1} is a distance function.

3.3 Body Force Due to Surface Tension Force

The model of Continuum Surface Force (CSF) [12] is employed to treat the surface tension force at the interface which interprets the surface tension force as a continuous effect across an interface rather than as a boundary condition on the interface. By using the level set function, body force due to surface tension force can be expressed as,

$$\frac{1}{We}\kappa\delta(d)\mathbf{n}=\frac{1}{We}\kappa(\phi)\delta(\phi)\nabla\phi \tag{22}$$

The curvature of the interface is evaluated from

$$\kappa(\phi)=-(\nabla\mathrm{g}\mathbf{n})=-\nabla\mathrm{g}\left(\frac{\nabla\phi}{|\nabla\phi|}\right) \tag{23}$$

The Dirac delta function is defined as

$$\delta_\alpha(\phi)=\frac{dH_\alpha(\phi)}{d\phi}=\begin{cases}0 & |\phi|>\alpha\\ \dfrac{1}{2\alpha}\left[1+\cos\left(\dfrac{\pi\phi}{\alpha}\right)\right] & |\phi|\le\alpha\end{cases} \tag{24}$$

3.4 Poisson Equation Solver

Briefly, we may write the Poisson equations for pressure as

$$\nabla\cdot\left(\frac{1}{\rho}\nabla p\right)=\frac{\nabla\cdot\mathbf{G}}{\Delta t} \tag{25}$$

$$\mathbf{G}=\begin{pmatrix}G_x\\G_y\\G_z\end{pmatrix}=\mathbf{u}+\Delta t\left(-(\mathbf{u}\cdot\nabla)\mathbf{u}+\frac{\mathbf{n}_{i\{i=x,z\}}}{Fr^2_{i\{i=x,z\}}}+\frac{1}{\rho}\left(\frac{1}{\mathrm{Re}}\nabla\cdot(2\mu D)+\frac{1}{We}\kappa(\phi)\delta(\phi)\nabla\phi\right)\right) \tag{26}$$

The Successive Over Relaxation (SOR) method has been used to solve the Poisson equation for pressure.

3.5 Smoothing of Interface

For immiscible two-phase fluids the density and viscosity can be expressed by the following equations

$$\rho_t+(\mathbf{u}\cdot\nabla)\rho=0 \tag{27}$$

$$\mu_t+(\mathbf{u}\cdot\nabla)\mu=0 \tag{28}$$

Since ρ and μ change sharply at the interface, conventional finite difference schemes will incur excessive numerical diffusion when solving equations (27) and (28). In order to overcome the difficulty, we will give the interface a finite thickness 2α and let ρ and μ vary smoothly at the interface. Therefore, the density ρ and viscosity μ can be expressed as follows.

$$H_\alpha(\phi)=\begin{cases}0 & \phi<-\alpha\\ (\phi+\alpha)/(2\alpha)+\sin(\pi\phi/\alpha)/2\pi & |\phi|\le\alpha\\ 1 & \phi>\alpha\end{cases} \tag{29}$$

$$\rho(\phi)=\rho_{in}+(\rho_{out}-\rho_{in})H_\alpha(\phi) \tag{30}$$

$$\mu(\phi)=\mu_{in}+(\mu_{out}-\mu_{in})H_\alpha(\phi) \tag{31}$$

In the present numerical simulations, we took $\alpha=3\Delta x/4$.

3.6 Time Stepping Strategy

Since the scheme is explicit, a CFL condition must be satisfied in order to ensure stability. In many cases, the gravitational force and surface tension terms are sufficiently stiff to require a more

restricted time step than a standard CFL estimate would predict. We have augmented the standard CFL estimate by setting

$$\Delta t_s = \sqrt{(\rho_{out} + \rho_{in})\frac{We}{8\pi Fr^2}}\Delta x^{3/2} \tag{32}$$

$$\Delta t_v = \min\left(\frac{3}{14}(\mathrm{Re})\Delta x^2/\mu\right) \tag{33}$$

$$\Delta t_c = \min\left(\frac{\Delta x}{|u|}\right) \tag{34}$$

$$\Delta t^{n+1} = c\min(\Delta t_s, \Delta t_v, \Delta t_c) \tag{35}$$

The constant, c, is a safety factor to be determined experimentally. We have taken $c = 1/2$.

Moreover, we briefly summarize the present strategy. The level set formulation of Eulerian interface capturing methods was applied to analyze the free surface motion of the liquid bridge. The Navier-Stokes equations in primitive variable formulations were solved on a staggered grid by the method of lines. The advection terms were discretized by the QUICK method and the other terms by the central finite difference method or the collocation difference method except for the body force, and a second-order Adams-Bashforth method was used as the time integration scheme. The Poisson equations were solved by means of the Successive Over - Relaxation (SOR) approach. The model of Continuum Surface Force (CSF) was employed to treat the surface tension force at the interface.

4 RESULTS AND DISCUSSION

4.1 Effects of Vibrations on ΔT_{cr} for a Silicone Oil Bridge

The test section was subjected to small vibrations by moving the translation stage in the x-direction over a distance of 10 cm at a constant speed of 2.67 cm/s. The acceleration levels recorded and their power spectra are shown in Figures. 4.1 and 4.2. Under these vibrations, the temperature difference between the upper and lower disks of a silicone oil bridge was increased gradually. Figures 4.3 and 4.4 show the fluid temperature fluctuations in the silicone oil bridge with an aspect ratio (H/D) of 0.95 for no vibration and with vibrations applied, respectively. The values of critical ΔT were determined following the same procedure as described in our previous report.[6]

The corresponding power spectra of the temperature oscillation data are shown in Figures 4.5 and 4.6, respectively. The oscillation frequency for this liquid bridge was 1.0 Hz, and peaks in the spectra are seen in both cases. In the vibration case, additional peaks are evident at harmonics of various vibration frequencies.

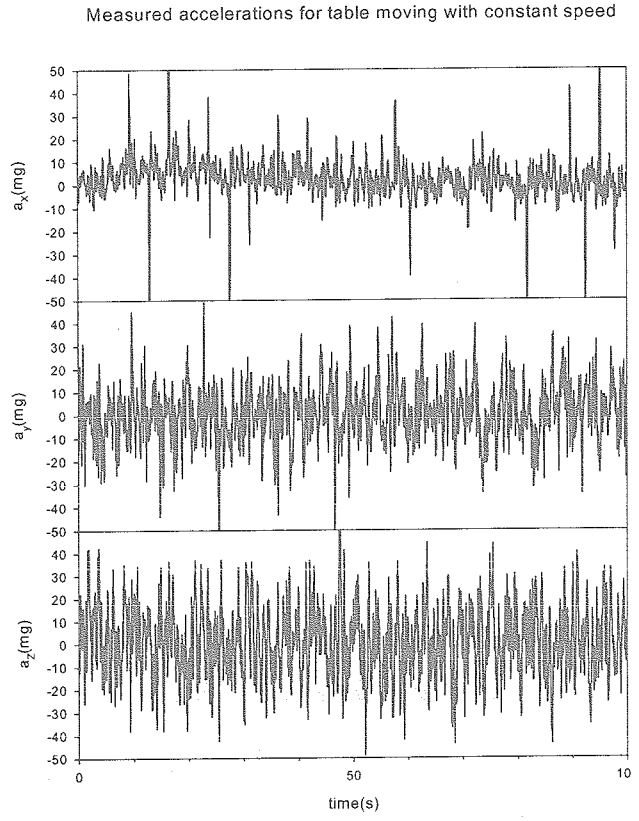

Figure 4.1 Acceleration levels measured on a translation stage moving at a constant speed

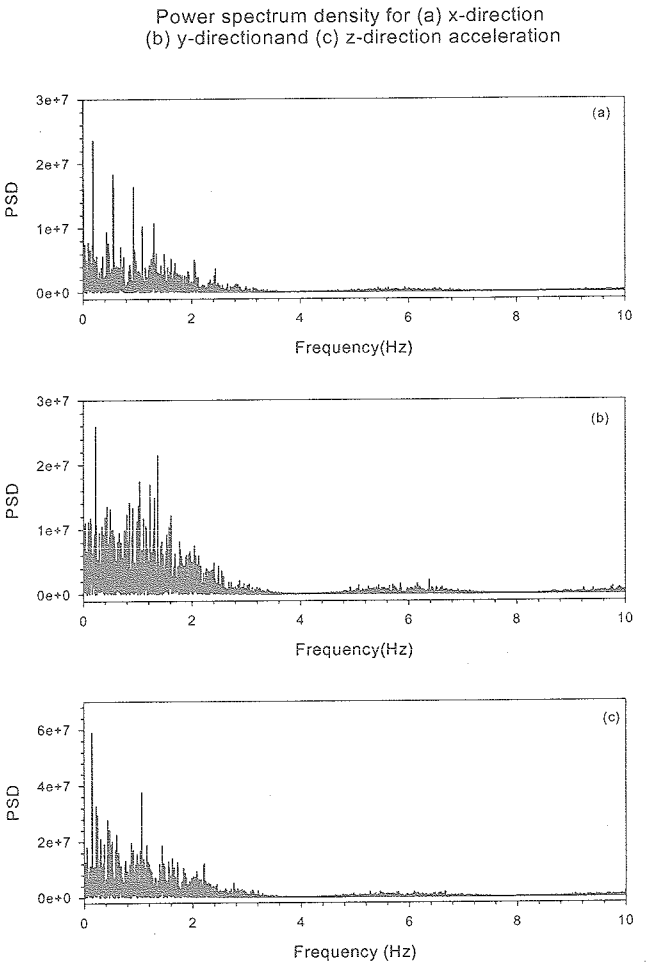

Figure 4.2 Power spectra of acceleration data shown in Fig. 4.1

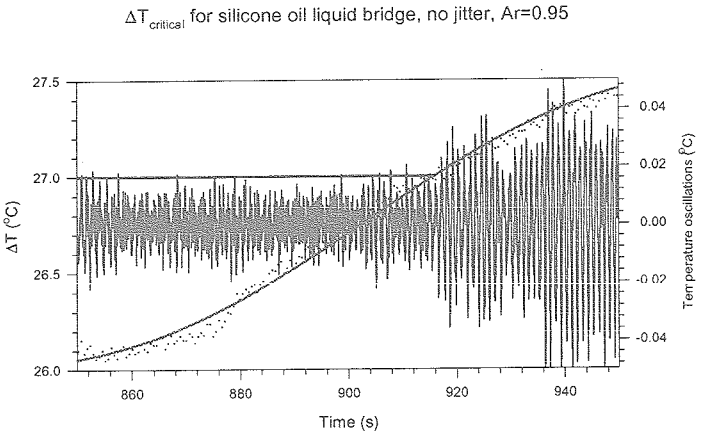

Figure 4.3 Onset of oscillatory Marangoni convection in a silicone oil bridge of 7 mm diameter and an aspect ratio = 0.95 for no vibration case

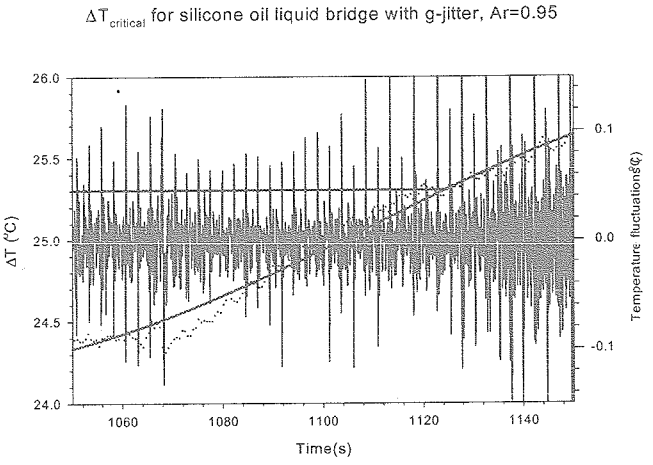

Figure 4.4 Onset of oscillatory Marangoni convection in a silicone oil bridge of 7 mm diameter and an aspect ratio = 0.95 for vibration case

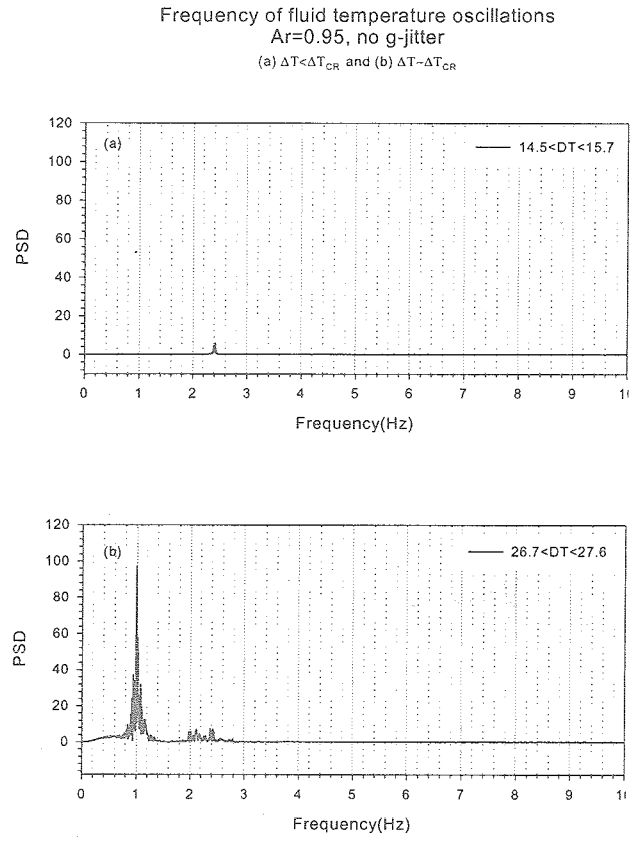

Figure 4.5 Power spectra of liquid temperature oscillations in a silicone oil bridge of 7 mm diameter and an aspect ratio = 0.95 for no vibration case

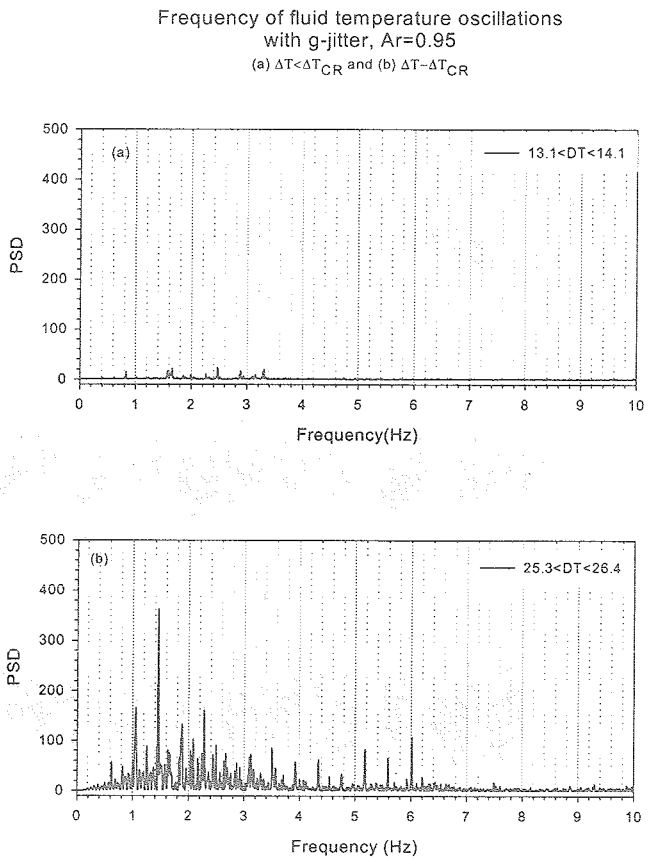

Figure 4.6 Power spectra of liquid temperature oscillations in a silicone oil bridge of 7 mm diameter and an aspect ratio = 0.95 for vibration case

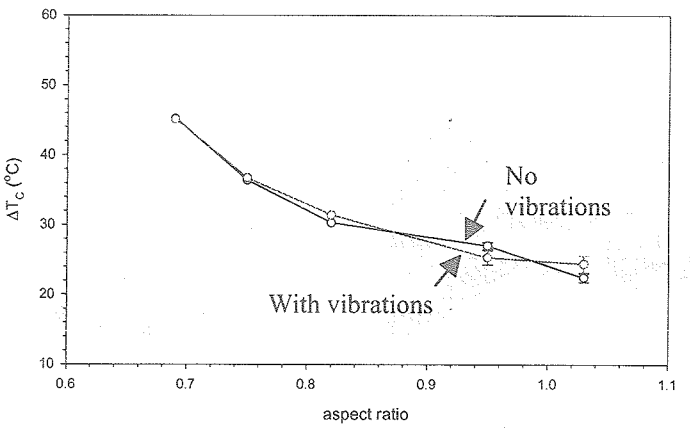

Figure 4.7 Effect of external vibrations on the critical temperature difference data obtained in a 5 cSt silicone oil bridge of 7 mm disk diameter

Figure 4.7 shows the effect of external vibrations on the critical temperature difference data for 5 cSt silicone oil. It is evident from this figure that the external vibrations had a negligible effect on the critical temperature difference for different aspect ratios.

4.2 Surface Oscillations of a Silicone Oil Bridge

The amplitude of surface oscillations was also determined for a silicone oil bridge of D = 7.0 mm, H = 3.5 mm, and an aspect ratio (H/D) of 0.5 as shown in Figures 4.8 and 4.9. A high-speed video camera at a frame speed of 124 fps was used with a pixel resolution of 2.0 μm. The liquid bridge was placed on a translation stage moving horizontally at a constant speed. Without any vibrations applied (Fig. 4.8), the peak-to-peak surface oscillation amplitude was less than 4 μm. Since the pixel resolution was 2 μm, the amplitude of 4 μm can be considered to represent slightly more than the background noise in the images recorded. On the other hand, the liquid bridge surface responded to small vibrations with irregular oscillations of varying amplitudes depending on the temperature difference between the upper and lower disks. The surface did not follow a simple to-and-fro motion but showed a complex response to the applied vibrations.

In Figure 4.9, the peak-to-peak amplitudes of the oscillating liquid bridge surface are plotted for different temperature differences. In the absence of any temperature gradient, $\Delta T = 0$, the peak-to-peak oscillation amplitude increased from about 20 μm at a distance of 100 μm below the hot corner to 50 μm at a distance of 500 μm below. By decreasing the lower disk temperature while keeping the upper disk temperature constant, the surface temperature of the liquid bridge below the hot corner also decreased but surface tension increased. The increase in surface tension had a stabilizing effect on the oscillation of the liquid bridge surface, therefore the peak-to-peak amplitude decreased for an increasing ΔT less than ΔT_{cr}. In Figure 4.9, the peak-to-peak amplitude for $0 < \Delta T < \Delta T_{cr}$ was reduced to about a half of that obtained for $\Delta T = 0$. The stabilizing effect was more pronounced further below the hot corner where the local temperature was lower and surface tension higher.

Increasing ΔT to ΔT_{cr} at which transition to oscillatory convection occurred caused an abrupt increase in the peak-to-peak amplitude although the average temperature of the liquid bridge was lower and therefore the stabilizing effect of surface tension was greater. Two different measurements at the onset of oscillatory flow are shown in Figure 4.9. Interestingly, further increasing the temperature difference above the critical value, $\Delta T > \Delta T_{cr}$, caused the peak-to-peak surface oscillation amplitude to significantly decrease below the hot corner, although it did not change at distances within about 30 μm below the hot corner.

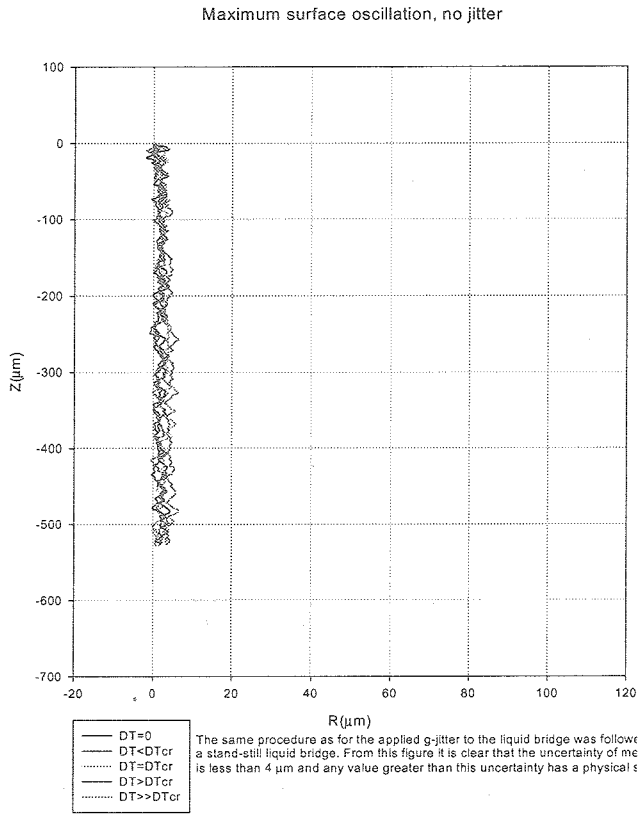

Figure 4.8 Peak surface oscillation amplitude for different temperature differences

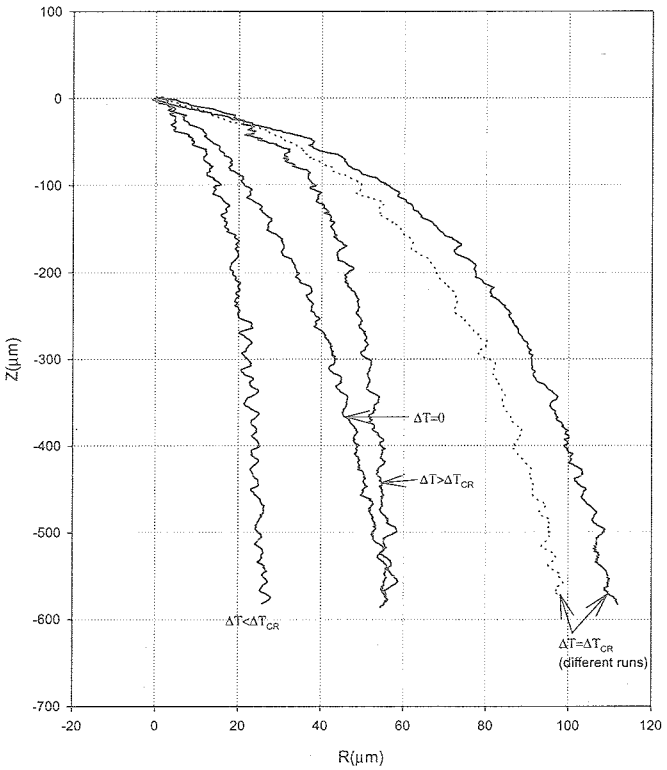

Figure 4.9 Effect of external vibrations on the peak surface oscillation amplitude

The reason for the peculiar dependence of the surface oscillation amplitude on the imposed temperature difference described above is not clear at present. The mechanism of transfer and conversion of vibration energy to surface oscillation as well as its relation to flow/temperature oscillation at the onset of oscillatory Marangoni convection need to be investigated further in the future, as Kamotani et al. (1984)[13] have suggested the existence of triple coupling among surface, velocity and temperature oscillations at the onset of oscillatory Marangoni convection in a non-vibrated liquid bridge. Although the characteristic frequencies are quite different among the imposed vibrations, flow/temperature oscillations, and the vibration-induced surface oscillations, there may be a link between Kamotani et al.'s triple coupling mechanism and an amplification of the vibration-induced surface oscillations presented in this work.

The effect of external vibrations arising from a DC motor running near the stationary test section on the liquid bridge surface is shown in Figure 4.10. The raw and smoothed surface position data for a silicone oil bridge of an aspect ratio (H/D) = 0.5 and a reduced volume ratio (minimum liquid bridge diameter to disk diameter ratio = 0.75) both showed an oscillation frequency of about 15 Hz.

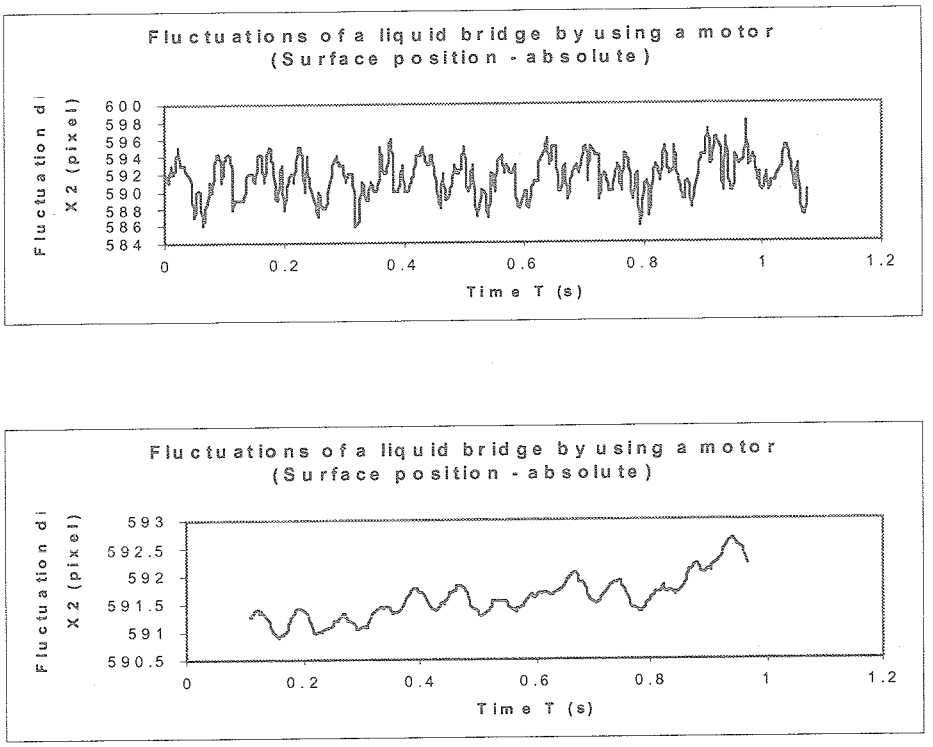

Figure 4.10 Surface oscillation data for a liquid bridge of diameter ratio = 0.75 due to an external vibration generated by a DC motor

5. NUMERICAL RESULTS

5.1 Computational Domain

The 3-D problems were solved in the following domain shown in Figure 5.1.

$$\Omega = \{(x,y,z) \mid 0 \le x \le 4R,\ 0 \le y \le 4R,\ 0 \le z \le R\}$$

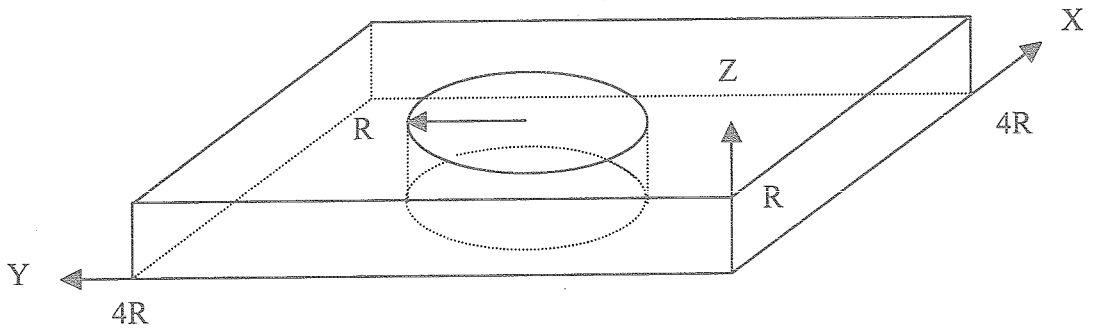

Figure 5.1 Schematic of 3-D computational domain for a liquid bridge simulation

5.2 Analyses of 3 - D Simulation Results

Our computations simulated the motion of an isothermal liquid bridge, and attention was paid to the displacement of the free surface of the liquid bridge. The key parameters were the

density ratio, ρ_{air}/ρ_l, viscosity ratio, μ_{air}/μ_l, Weber number $We = \rho_l U_\infty^2 D/\sigma$, and Reynolds number $\mathrm{Re} = \rho_l U_\infty D/\mu_l$. The physical properties and geometric parameters used to determine the above dimensionless parameters can be found in Table 5.1.

Table 5.1. Physical properties and geometric parameters

			5 cSt silicone oil	Air
Density	ρ	[kg/m^3]	915	1.226
Viscosity	μ	[kg/ms]	4.575×10^{-3}	1.78×10^{-5}
Surface tension	σ	[N/m]	1.97×10^{-2}	—
Diameter of disks	D	[m]	7×10^{-3}	
Height of liquid bridge	H	[m]	3.5×10^{-3}	
Gravity	g	[m/s^2]	9.81	

The initial shape of the liquid bridge is shown in Figure 5.2, which was a straight cylinder and would deform under gravity and applied vibrations in the vertical and horizontal directions, respectively. Both the liquid bridge and the surrounding air were at rest initially. The applied acceleration level in the horizontal direction was 20 mg.

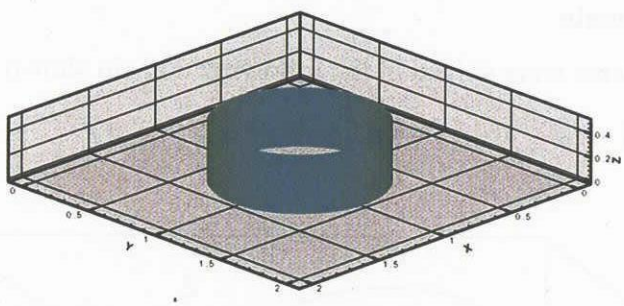

Figure 5.2 Initial shape of a 3-D liquid bridge

The evolution of the liquid bridge shape due to vibrations and surface tension under gravity can be found in Figures 5.3(a)-(b). These figures show the predicted liquid bridge shape as viewed at an angle of 30 degrees above the ground. The upper and lower boundaries of the liquid bridge were fixed completely to the upper and lower disks, respectively. The deformation near the lower disk was outward and that near the upper disk was inward, which are consistent with the increase in pressure near the lower disk and decrease of pressure near the upper disk due to the effect of gravity. We can also view the liquid bridge from a horizontal angle and compare the shapes predicted at

dimensionless times, t = 1.0 and t = 3.8, as shown in Figure 5.4(a)-(b). Because the applied vibrations in the horizontal direction were so small, the shapes appear to be the same between Figure 5.4(a) and (b), however, the surface was oscillating as described below.

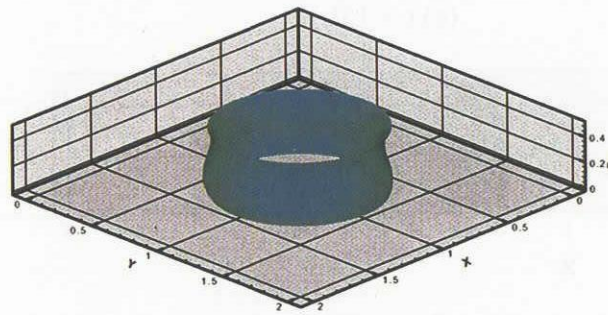

(a) t = 1.0

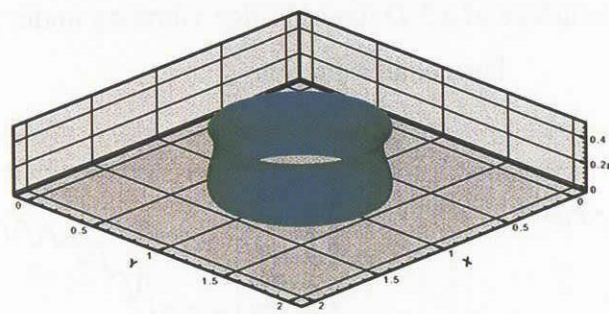

(b) t = 3.8

Figure 5.3 Evolution of a free surface of a liquid bridge oscillating due to a small horizontal vibration under gravity

To quantify the motion of the liquid bridge surface due to small vibrations applied in the horizontal direction, simulations were conducted for a liquid bridge under microgravity using a 51 x 51 x 51 mesh. The applied vibration frequency was 15 Hz, and the acceleration level in the horizontal direction was 18-mg. Three monitoring points on the surface of the liquid bridge were taken at heights 4/H, H/2, 3H/4, from the bottom disk. Figure 5.5 shows the evolution of the surface position at the three monitoring heights. At all heights, the liquid bridge surface was predicted to oscillate in the horizontal direction with a frequency of about 15Hz, which was in good agreement with that obtained experimentally on the ground and previously shown in Fig. 4.10.

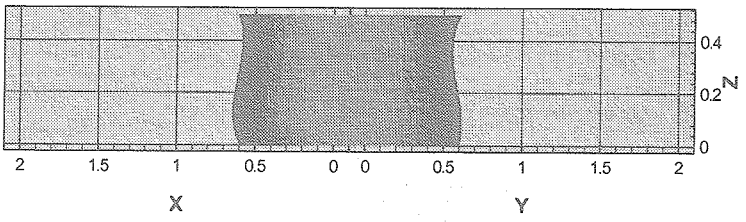

(a) t = 1.0

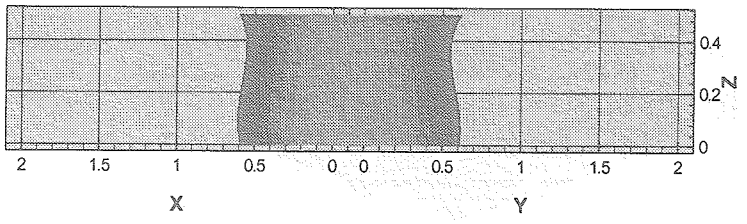

(b) t = 3.8

Figure 5.4 Evolution of a free surface of a 3-D liquid bridge vibrating under gravity and small horizontal vibration

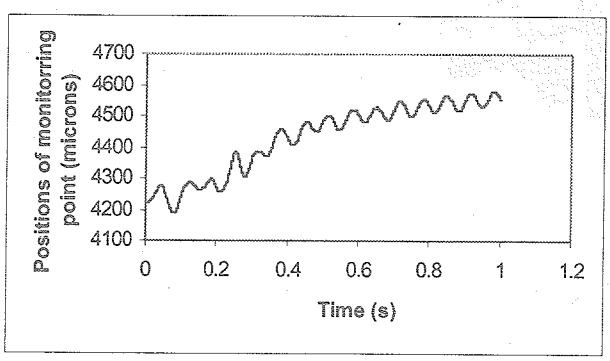

(a) Observation point: 3H/4

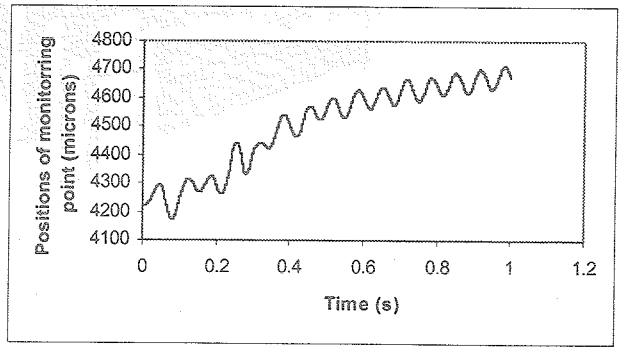

(b) Observation point: H/2

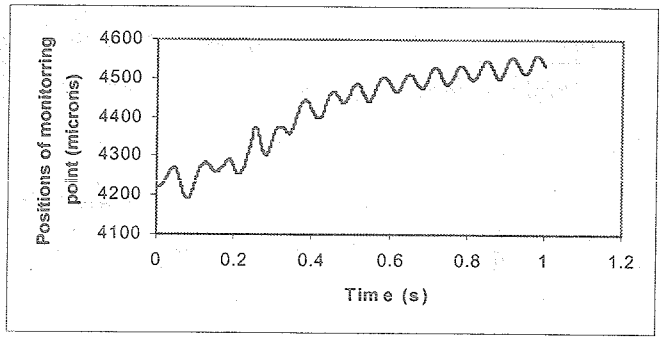

(c) Observation point: H/4

Figure 5.5 Predicted oscillations of a liquid bridge surface driven by small horizontal vibrations

6. CONCLUSIONS

The effects of small vibrations on Marangoni convection were investigated using a liquid bridge of 5 cSt silicone oil with a disk diameter of 7.0 mm, and an aspect ratio (H/D) close to 0.5. Experiments were performed to determine the critical temperature difference data for no vibration case and with small vibrations applied. The surface oscillation amplitude was also determined experimentally. A 3-D numerical simulation model was also developed using a level set algorithm to predict the surface oscillations of an isothermal liquid bridge.

The experimental results have shown that the effect of small vibrations on the onset of oscillatory flow is small since the critical temperature difference data for different aspect ratios were not affected by the vibrations. This is consistent with the results obtained for acetone bridges reported in the previous year.

The peak amplitudes of surface oscillations decreased as the disk temperature difference was increased and the average liquid temperature decreased. This can be attributed to an increase in surface tension which stabilizes the liquid bridge surface. The surface oscillation amplitude, however, showed an abrupt increase at the onset of oscillatory Marangoni convection, and then a decrease as the temperature difference was further increased above the critical value. The reason for this variation in the surface oscillation amplitude with the temperature difference is unclear and needs to be investigated further.

To clarify the surface oscillation phenomena induced by external vibrations, experiments and numerical simulations were conducted for an isothermal silicone oil bridge of 7.0 mm diameter. By subjecting the bridge to small random vibrations, the surface oscillation frequency could be clearly determined. The computational results have also shown a similar surface oscillation frequency.

7. NOMENCLATURE

A	Vibration amplitude
d	Normal distance to the interface
D	Diameter of the upper and lower disks
f	Vibration frequency
$\mathbf{F}$	Propagating speed of a closed moving interface normal to itself
FGX	Body force in horizontal direction
Fr	Froude number
g	Gravity
g_x	Acceleration in horizontal direction
$\bar{L}$	Characteristic length
$\mathbf{n}$	Unit outward normal vector at the interface
$\mathbf{n}_{i(i=x,z)}$	Unit vector in x and z direction, respectively

p	Pressure
R	Radius of the upper and lower disks
Re	Reynolds number
t	Time
Δt	Time step
$\mathbf{u}$	Velocity vector
U_∞	Characteristic velocity
We	Weber number
Δx	Grid increase in x direction
α	Thickness of the interface
δ	Dirac delta function
ϕ	Level set function
Γ	A closed moving interface
κ	Curvature of the interface
μ	Viscosity
μ_l	Viscosity of liquid
μ_{in}	Viscosity ratio
μ_{out}	Viscosity ratio
ρ	Density
ρ_l	Density of liquid
ρ_{in}	Density ratio
ρ_{out}	Density ratio
σ	Surface tension
ω	Angular frequency in horizontal direction
Ω	Region that a closed moving interface enclosed

REFERENCES

1. F. Preisser, D. Schwabe, and A. Scharmann, "Steady and oscillatory thermocapillary convection in liquid columns with free cylindrical surface", J. Fluid Mech., 126, 545 (1983).
2. R. Velten, D. Schwabe, and A. Scharmann, "The periodic instability of thermocapillary convection in cylindrical liquid bridges", Phys. of Fluids A, 3(2), 267 (1991).
3. M. Kawaji, F. Otsubo, and S. Yoda, "Transition to oscillatory Marangoni convection in liquid bridges of intermediate Prandtl number", Paper NHTC2000-12200, Proc. of the 34th National Heat Transfer Conference, Pittsburgh, Pennsylvania, August 20-22, 2000.
4. M. Kawaji, F. Otsubo, S. Simic, and S. Yoda, "Transition to oscillatory Marangoni convection in liquid bridges of intermediate Prandtl number", Annual Report on Marangoni Convection Modeling Research, NASDA Technical Memorandum, National Space Development Agency of Japan, 107-132, (2001).
5. N. Ichikawa, M. Misawa, and M. Kawaji, "Resonance behavior of liquid bridge caused by small vibration", Proc. of 4th International Conference on Multiphase Flow, New Orleans,

Louisiana, USA. May 27 – June 1, 2001.

6. M. Kawaji, M. Nasr-Esfahany, and S. Simic, "Investigation of Horizontal Vibrations on Marangoni Convection in a Liquid Bridge", Annual Report on Marangoni Convection Modeling Research, NASDA Technical Memorandum, National Space Development Agency of Japan, 109-128 (2002).
7. S. Osher and J.A. Sethian, "Fronts propagating with curvature-dependent speed: Algorithm based on Hamilton-Jacobi formulation", J. Compt. Phys., 79, 12 (1988).
8. R. Q. Liang and N. Satofuka, "Numerical solutions of moving interface behavior in incompressible gas-liquid two-phase flow using level set approach", J. JSME, 64, 42 (1998).
9. R. Q. Liang and N. Satofuka, "A front capturing method for droplet motions involving multi-phases", CFD Journal, ISSN 0918-6654, 470 (2001).
10. R. Q. Liang and N. Satofuka, "Numerical simulations of droplet and bubble flows using fast level set method", CFD 731(2000)(Springer).
11. M. Sussman, P. Smereka, and S. Osher, "A level set approach for computing solutions to incompressible two-phase flow", J. Compt. Phys., 114, 146 (1994).
12. J.D. Brackbill, D.B. Kothe, and C. Zemach, "A continuum method for modeling surface tension", J. Compt. Phys., 100(2), 335 (1992).
13. Y. Kamotani, S. Ostrach, and M. Vargas, "Oscillatory thermocapillary convection in a simulated float-zone configuration", J. Crystal Growth, 66, 83 (1984).